Identification of polymer materials in electronic packages using FTIR-ATR spectroscopy and SIMCA chemometric analysis

Measurement Science and Technology

OPEN ACCESS

RECEIVED
22 March 2026

REVISED
9 June 2026

ACCEPTED FOR PUBLICATION
14 July 2026

PUBLISHED
4 August 2026

PAPER

Identification of polymer materials in electronic packages using FTIR-ATR spectroscopy and SIMCA chemometric analysis

Junbo Yang*, Yuhan Gao*, Yi Deng, Karthik Deo, Dalei Yang, Weichen Zhao, Kewei Shou and Seungbae Park

Mechanical Engineering Department, Binghamton University, New York 13850, United States of America
* Authors to whom any correspondence should be addressed.

E-mail: jyang151@binghamton.edu and ygao18@binghamton.edu

Keywords: FTIR-ATR spectroscopy, SIMCA classification, principal component analysis (PCA), polymer identification, electronic packaging materials, thermal interface materials

Abstract

Accurate identification of polymer materials used in electronic packaging is essential for assembly control, reliability analysis, and counterfeit material detection. However, polymer materials embedded in electronic assemblies are often difficult to identify because they are present in small quantities and consist of heterogeneous composites containing polymer matrices and inorganic fillers. In this study, a measurement framework is developed for identifying polymer materials in electronic packages using Fourier transform infrared spectroscopy with attenuated total reflectance (FTIR-ATR) combined with chemometric analysis. Representative packaging polymers including four underfill materials, two thermal interface materials, and one die attach (DA) adhesive were used to build the classification library. Cross-sectioned package samples were analyzed using micro-ATR FTIR spectroscopy in the fingerprint region (650–1800 cm^{-1}), and baseline correction was applied before multivariate analysis. Principal component analysis was used for dimensionality reduction and visualization of spectral clustering, while Soft Independent Modeling of Class Analogy (SIMCA) was used for supervised class modeling and unknown rejection. Using spectra collected from independently prepared package samples, SIMCA correctly classified most test spectra from the modeled library and rejected an external DA material (DA2) as unknown. The results demonstrate that the FTIR-ATR and SIMCA approach provides a rapid and reliable method for identifying polymer materials in electronic packaging and can support applications such as failure analysis, reliability modeling, and material verification.

1. Introduction

Polymer materials play an essential role in modern electronic packaging systems by providing mechanical support, environmental protection, and thermal management for semiconductor devices. Common polymer materials used in electronic packaging include epoxy-based underfills, die attach adhesives (DA), and thermal interface materials (TIMs), which improve reliability by redistributing thermomechanical stress and enhancing heat dissipation [1–3].

Underfill materials are widely used in flip-chip packaging to mitigate the coefficient of thermal expansion (CTE) mismatch between silicon chips and organic substrates [4–7]. By redistributing stress away from solder joints and coupling the chip–underfill–substrate structure, underfills can substantially improve fatigue life and long-term package reliability [8–10]. In advanced packaging, underfill selection is further constrained by competing failure modes (e.g. solder fatigue, die cracking, and delamination), making the correct identification of underfill families and formulations important when documentation is incomplete.

Underfills are typically formulated as epoxy resin matrices heavily filled with fused silica (SiO_2) and supplemented with additives (e.g. catalysts, coupling agents, adhesion promoters) to control viscosity, flow, cure kinetics, modulus, moisture uptake, and CTE. Because the composite thermomechanical

properties depend strongly on filler–matrix design, polymer composite literature also emphasizes that filler type/volume fraction significantly affects effective modulus and CTE [11, 12].

Polymer adhesives and thermally conductive composites are also widely applied in electronic assemblies. In DA applications, epoxy adhesives are used to bond dies to substrates, and conductive formulations (e.g. silver-filled epoxies) are actively engineered for electrical/thermal conduction and reliability constraints such as silver migration and interfacial stability [13]. For thermal management, TIMs (often silicone/PDMS-ilicone/PDMS management, TIMs (often sWK' as silver migration and interfacial stabilitnterfacial stabiliter type/volume fraction significantly affects effective modulus and CTe modulus and CTill families and formulad in electunderfills, DA adhesives, and TIMs strongly influence package reliability and thermal performance, accurate identification of packaging polymers is important for failure analysis, reliability assessment, and process control [14–17].

In many practical situations, the specific polymer materials used in electronic products are unknown because of proprietary formulations or incomplete documentation. This lack of information complicates reliability modeling and finite-element simulations of electronic packages, which require accurate material properties as inputs [18, 19].

Identification of cured polymer materials extracted from electronic packages presents several practical challenges. First, the available sample quantity is typically small and embedded in complex assemblies. Second, curing forms cross-linked thermoset networks that are insoluble and not melt-processable, limiting the applicability of solution-based or bulk reprocessing methods. Third, packaging polymers are heterogeneous composites containing inorganic fillers and additives, producing spatial and compositional non-uniformity at the scales probed by micro-analysis methods.

A range of analytical techniques have therefore been used for polymer characterization, including nuclear magnetic resonance (NMR), pyrolysis-gas chromatography/mass spectrometry (Py-GC/MS), thermogravimetric analysis (TGA), and infrared spectroscopy. Solid-state NMR has been repeatedly used to study cure extent, cross-linking structure, and formulation components in epoxy systems, including thermosets and commercial multicomponent products [20]. Py-GC/MS is a powerful approach for identifying polymers/additives and has been explicitly demonstrated for cured epoxy resins and complex polymer mixtures [21]. TGA is widely used to evaluate thermal stability and (in filled systems) inorganic residue/filler fraction [22]. While these techniques provide valuable structural and compositional information, they can require specialized instrumentation, more extensive preparation, or workflows that are less convenient for rapid screening of small extracted packaging samples.

Fourier transform infrared spectroscopy (FTIR) provides a rapid and non-destructive method for identifying organic materials based on molecular vibrational absorption spectra. When combined with attenuated total reflectance (ATR), FTIR enables direct analysis of solid samples with minimal preparation. ATR-FTIR operates by generating an evanescent infrared wave at the interface between a high-refractive-index crystal and the sample surface, allowing surface-sensitive spectral measurements. The theoretical principles of ATR spectroscopy were first described in early studies of total internal reflection and infrared absorption. Subsequent research demonstrated that the effective path length of ATR measurements depends on optical parameters such as refractive index, wavelength, and incident angle [23, 24].

Because FTIR spectra of complex polymer systems can contain overlapping peaks and baseline variation (e.g. due to fillers, scattering, and contact variability), chemometric techniques are widely used to extract robust classification information from spectral datasets. Principal component analysis (PCA) is a common dimensionality-reduction technique that transforms correlated spectral variables into orthogonal principal components capturing the majority of variance in the data [25, 26]. For classification and screening problems, Soft Independent Modeling of Class Analogy (SIMCA) is a widely used class-modeling method that builds a PCA model for each class and can accept or reject unknown samples based on distance/leverage criteria. At the same time, SIMCA performance depends on model design, training representativeness, and decision limits, and comparative studies note that alternative discriminant classifiers may outperform SIMCA in some settings, reinforcing the need for transparent validation and uncertainty-aware deployment [27–29].

Recent FTIR and ATR-FTIR studies have increasingly combined chemometric or machine-learning analysis with infrared spectra for polymer recognition, spectral-library matching, and material classification [30–41]. These include ATR-FTIR/PCA-based recognition of polyamide materials [34], ATR-FTIR with multivariate monitoring of polymer processing [37], automated micro-FTIR spectral matching for microplastics [38], FTIR imaging protocols for rapid microplastic identification [39], ATR-FTIR chemometrics for rapid identification of multiple microplastic types [40], and machine-learning classification of FTIR fingerprint-region spectra [41]. These studies demonstrate the broader value of infrared spectroscopy combined with multivariate modeling, but most focus on bulk polymers,

Table 1. Material library used in this study.

Material	Manufacturer	Material type
UF1	United Adhesives Inc. UF1230	Underfill encapsulant
UF2	United Adhesives Inc. EP1641	Underfill encapsulant
UF3	YINCAE SMT88U	Underfill encapsulant
UF4	Shin-Etsu SMC-375TGSF5	Underfill encapsulant
TIM1	Shin-Etsu X-23–7762	Thermal interface material
TIM2	Honeywell PTM7900	Thermal interface material
DA1	Loctite 8700 K	Die attach adhesive
DA2	Loctite QMI538NB	Die attach adhesive

environmental microplastics, pharmaceutical/chemical products, or process-monitoring datasets rather than polymer materials measured directly from electronic-package cross-sections. The objective of this study is therefore to develop a rapid identification method for polymer materials used in electronic packaging by combining FTIR-ATR spectroscopy with SIMCA chemometric classification.

2. Materials and methods

2.1. Polymer materials and package preparation

Representative polymer materials commonly used in electronic packaging were selected to evaluate the proposed identification methodology. These materials were chosen to cover the major classes of polymer systems used in semiconductor packaging, including underfill encapsulants (UF), TIMs, and DA adhesives.

Seven polymer formulations were used to build the classification library as shown in table 1: four epoxy-based UF (UF1–UF4), two TIMs (TIM1 and TIM2), and one DA adhesive (DA1). A second DA adhesive, DA2, was not included as a modeled class. Instead, DA2 was reserved as an external unknown challenge material to evaluate whether the SIMCA models could reject a spectrum that did not belong to any of the seven modeled classes. The TIMs consisted of one phase-change material and one thermal grease. These material categories represent the most frequently used polymer systems for mechanical reinforcement, thermal management, and chip attachment in electronic packaging assemblies.

Underfill materials are typically epoxy-based composites formulated with silica fillers and various additives to control rheological behavior, curing kinetics, and mechanical properties. DA adhesives are polymer bonding materials used to attach semiconductor dies to substrates or lead frames, while TIMs are designed to reduce thermal resistance between electronic devices and heat dissipation components such as heat sinks.

To simulate realistic packaging conditions, test assemblies were fabricated using printed circuit boards as substrates and silicon blocks to represent semiconductor dies. Underfill materials were dispensed along the chip edges and allowed to flow beneath the chip through capillary action before curing.

After curing and assembly, cross-sections of the packages shown in figure 1 were prepared to expose the polymer materials for spectroscopic analysis. Because polymer materials in assembled electronic packages are typically present in very small quantities and are difficult to isolate from surrounding structures, the identification method must be capable of analyzing microscopic sample regions directly from the package. For this reason, FTIR-ATR microscopy was employed for spectral measurement.

The sampling procedure was adjusted according to the dispensing behavior of each material. Underfill materials were treated separately because capillary flow from the dispense side to the opposite side can produce spatial variation in resin/filler distribution. Therefore, underfill spectra were collected from multiple vertical and horizontal positions in the cross-section. DA1 and the TIM samples were prepared as polymer layers in package samples and measured from exposed cross-sectional regions. Because these layers were dispensed more uniformly than capillary underfill in the package geometry used here, inlet/outlet sampling was not required for DA1 and TIM1/TIM2. All measurements were performed on exposed polymer regions in package cross-sections using the same micro-ATR FTIR contact procedure.

2.2. FTIR-ATR measurements

Infrared spectrum of the polymer materials was obtained using FTIR equipped with an ATR microscope accessory. FTIR spectroscopy measures the absorption of infrared radiation associated with molecular vibrational modes within a material, producing characteristic spectral fingerprints that can be used for chemical identification. ATR-FTIR was selected in this study because it enables direct analysis of solid

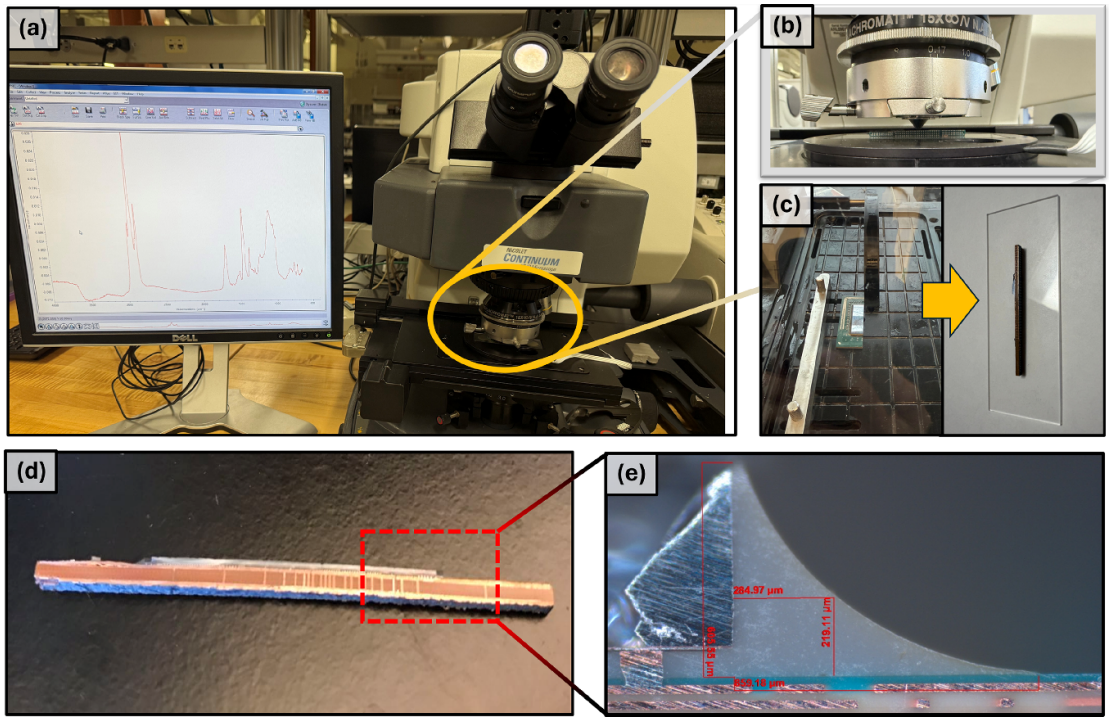

Figure 1. Electronic package cross-section and sampling location of the polymer layer for FTIR-ATR measurement. (a) Schematic of the FTIR-ATR measurement setup; (b) Photograph of the sample during measurement; (c) Sectioned electronic package sample; (d) Cross-sectional view of the package sample; (e) Enlarged view of the underfill region indicating the sampling location.

polymer samples with minimal sample preparation. In ATR measurements, an infrared beam undergoes total internal reflection inside a high-refractive-index crystal. At each reflection, an evanescent wave penetrates a short distance into the sample surface and interacts with molecular vibrations within the material, resulting in an absorption spectrum characteristic of the sample composition.

Spectral measurements were performed using a microscope-based FTIR spectrometer equipped with a Germanium ATR crystal. The high refractive index of the Germanium crystal provides a shallow penetration depth of the evanescent wave, which improves spatial resolution and allows localized measurement of small regions within the polymer material extracted from electronic packages. Prior to measurement, the sample surface was gently cleaned with isopropanol and dried using nitrogen gas to remove contaminants that could interfere with the infrared signal. Each sample was brought into contact with the ATR crystal under controlled pressure to ensure consistent optical coupling between the crystal and the sample surface.

Infrared spectra were acquired over a spectral range of 650–4000 cm^{-1} with a spectral resolution of 4 cm^{-1}, and 100 scans were averaged for each spectrum to improve the signal-to-noise ratio. Background spectra were collected before each measurement to compensate for atmospheric absorption and instrument response. Because polymer materials exhibit distinctive vibrational signatures in the infrared fingerprint region, the spectral range between 650 and 1800 cm^{-1} was selected for subsequent chemometric analysis. This region contains numerous absorption bands associated with functional groups present in epoxy-based polymer systems, including C–O and C–O–C stretching vibrations, aromatic ring modes, and Si–O–Si bands originating from silica fillers.

To account for potential heterogeneity within the polymer materials, multiple spectra were collected from different regions of each sample. The resulting spectral dataset was used for subsequent chemometric analysis.

2.3. Underfill spectrum collecting influence factors

Because dispensed underfill materials are heterogeneous mixtures consisting of resin systems and inorganic fillers, several factors may influence the infrared spectra collected from assembled packages. Understanding these factors is essential for establishing reliable procedures for spectral collection.

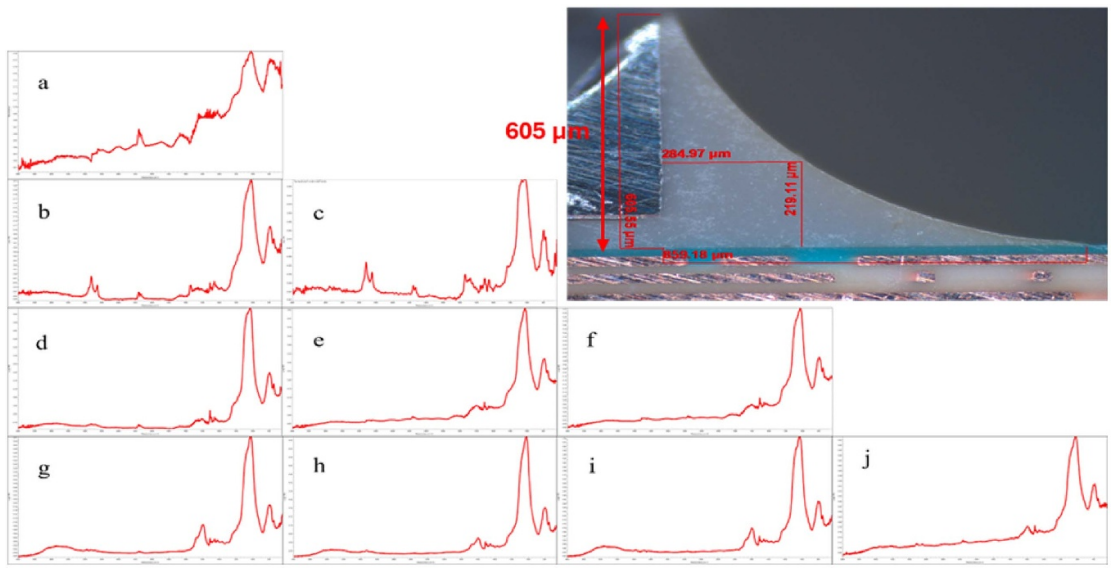

Figure 2. Detection working area chosen for filler settling influence study.

2.3.1. Filler settling

Underfill materials typically contain micron-sized silica fillers dispersed within an epoxy resin matrix. Although modern formulations are designed to minimize particle sedimentation, filler settling can still occur during storage or curing processes due to gravitational effects [42].

Since FTIR-ATR is a surface-sensitive technique that probes only a small region of the sample, the measured spectrum may depend on the local distribution of filler particles. To evaluate this effect, the detection area of the ATR microscope was adjusted between 50 × 50 μm^{-2} and 175 × 175 μm^{-2}, and spectra were collected from different vertical positions within the underfill cross-section shown in figure 2.

The total thickness of the cured underfill layer in the test assemblies was approximately 600 μm^{-1}. The cross-section was therefore divided into multiple vertical regions to evaluate spectral variations along the height direction. The results showed that spectra collected from different horizontal locations were generally similar, whereas spectra obtained at different heights exhibited noticeable variations due to differences in filler concentration.

These observations indicate that filler settling primarily affects the vertical distribution of spectral features within the underfill material. Consequently, infrared spectra should be collected from multiple vertical positions to ensure that the measured spectrum represents the overall material composition.

2.3.2. Filler movement during underfill flow

Another factor affecting spectral collection is the movement of filler particles during the underfill dispensing process. In conventional capillary underfill assembly, material is dispensed along one edge of the chip and flows beneath the chip through capillary action to fill the gap between the chip and the substrate [43].

During this flow process, filler particles may interact with solder bumps or other package features, leading to non-uniform filler distribution between the inlet region and the outlet region of the underfill flow path. Previous studies have reported that filler particles may accumulate near the inlet side due to interactions with the first row of solder bumps [44].

To investigate this effect, the underfill cross-section was divided into four regions corresponding to different positions along the flow direction. Spectra were collected from each region and averaged to obtain representative spectra for the inlet and outlet areas as shown in figures 3 and 4. The results showed that the spectral characteristics of the inlet region differed slightly from those of the outlet region, confirming that filler redistribution during capillary flow can influence the local composition of the underfill material.

2.3.3. Recommended spectrum collection strategy

Based on the observations discussed above, an appropriate spectral collection strategy is necessary to obtain representative infrared spectra from heterogeneous underfill materials extracted from electronic

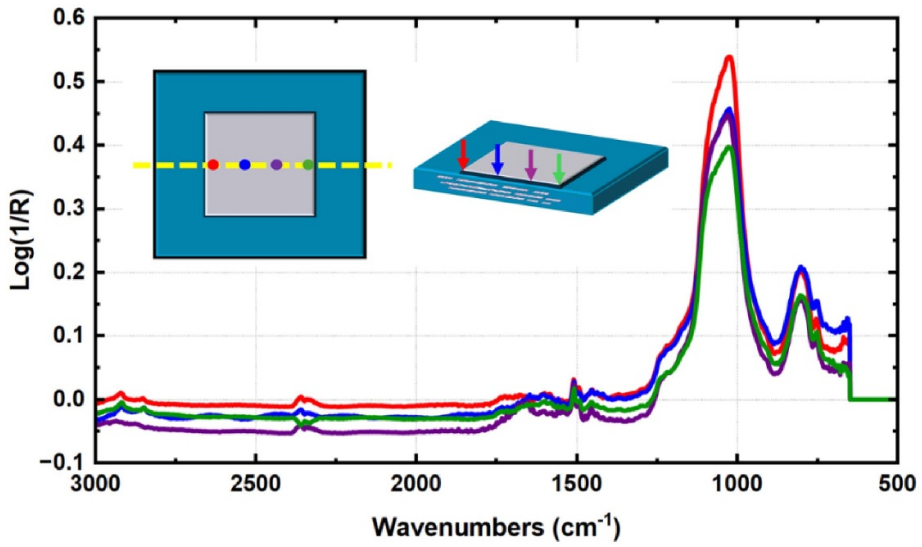

Figure 3. Section positions for filler movement influence study and average spectrum of each section.

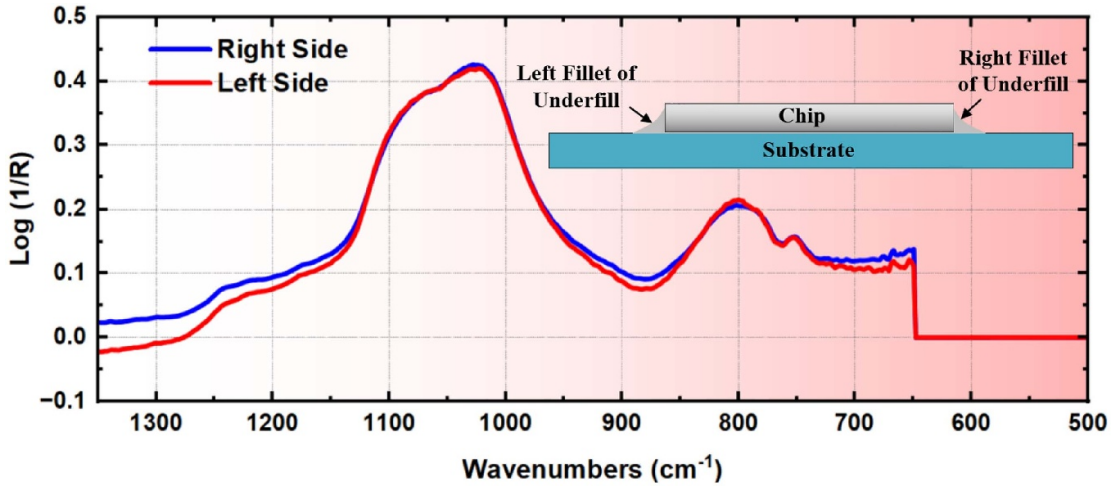

Figure 4. Average spectra of right and left side of one cross section.

packages. Because filler settling and flow-induced particle redistribution can lead to spatial variations in material composition, spectra must be collected from multiple regions of the sample to ensure that the measured dataset reflects the overall chemical characteristics of the material.

In this study, the underfill cross-section was divided into several vertical regions to account for potential variations caused by filler settling. In addition, spectra were collected from multiple horizontal locations corresponding to the inlet side, outlet side, and intermediate regions of the underfill flow path. Within each region, several spectra were acquired from different measurement locations and subsequently averaged to obtain representative spectra for chemometric analysis.

This positional collection rule was specifically applied to underfill because capillary flow and filler settling can create vertical and horizontal gradients. Spectra collected from the different underfill positions were included in the training dataset so that the class model captured within-class spatial variation. For DA and TIM samples, which were dispensed as more uniform layers in the package geometry used here, spectra were collected from exposed representative regions without inlet/outlet subdivision.

2.4. Spectral preprocessing

Prior to chemometric analysis, spectra were restricted to the fingerprint region from 650 to 1800 cm^{-1}. Baseline correction was performed on each dataset using The Unscrambler (version 10.4, Camo Process AS) to remove spectral offsets arising from scattering effects and instrumental response. No normalization, smoothing, derivative transformation, interpolation, outlier filtering, or ATR correction was applied.

The baseline-corrected spectra were mean-centered before PCA and SIMCA modeling. The same preprocessing sequence was applied to training spectra, test spectra, and the external unknown DA2 spectra.

3. Chemometric analysis

Because FTIR spectra consist of absorbance values measured at hundreds of wavenumbers, the resulting dataset is highly multivariate and contains significant correlations among variables. Direct interpretation of such high-dimensional spectral data can be difficult, particularly for heterogeneous materials such as cured underfills containing polymer matrices and inorganic fillers. To extract meaningful information from the spectra and perform reliable classification, multivariate statistical techniques were employed.

In this work, PCA was first applied to reduce the dimensionality of the FTIR spectral dataset and to visualize clustering patterns among different polymer materials. Subsequently, SIMCA was used as a supervised classification method to identify unknown polymer materials.

3.1. PCA

PCA is a widely used multivariate statistical technique for reducing the dimensionality of complex datasets while retaining the majority of the original information. PCA transforms correlated variables into a new set of orthogonal variables called principal components.

Let the FTIR spectral dataset be represented by the matrix

$$X = \begin{bmatrix} x_{11} & x_{12} & \cdots & x_{1p} \\ x_{21} & x_{22} & \cdots & x_{2p} \\ \vdots & \vdots & \ddots & \vdots \\ x_{n1} & x_{n2} & \cdots & x_{np} \end{bmatrix} \tag{1}$$

where n is the number of spectra and p is the number of spectral variables corresponding to the measured wavenumbers.

Prior to PCA, the dataset was mean-centered to remove systematic offsets:

$$B = X - \mathbf{1}\bar{x}^{\mathrm{T}} \tag{2}$$

where $\bar{x}$ represents the mean spectrum of the dataset and $\mathbf{1}$ is a column vector of ones.

The covariance matrix of the spectral dataset is then calculated as

$$C = \frac{1}{n-1} B^{\mathrm{T}} B. \tag{3}$$

The principal components are obtained by solving the eigenvalue problem

$$Cu_k = \lambda_k u_k \tag{4}$$

where u_k represents the eigenvector corresponding to the k-th principal component and λ_k is the associated eigenvalue.

The PCA score vector is calculated as

$$t_k = Bu_k. \tag{5}$$

The spectral dataset can therefore be approximated using the PCA model

$$X = TP^{\mathrm{T}} + E \tag{6}$$

where T is score matrix, P is loading matrix and E is residual matrix.

The cumulative explained variance for the first m principal components is calculated as

$$\eta_m = \frac{\sum_{k=1}^{m} \lambda_k}{\sum_{k=1}^{p} \lambda_k} \times 100\%. \tag{7}$$

In this study, PCA was applied to the FTIR spectra in the fingerprint region to evaluate clustering behavior among different polymer materials and to determine the number of principal components used for subsequent SIMCA modeling.

3.2. SIMCA classification method

While PCA provides visualization of spectral similarities, it does not directly classify unknown samples. Therefore, the SIMCA method was used for supervised classification of polymer materials.

In SIMCA, a separate PCA model is constructed for each material class g. For a given class, the spectral matrix is expressed as

$$X_g = T_g P_g^T + E_g \tag{8}$$

where T_g is score matrix of class g, P_g is loading matrix of class g and E_g is residual matrix.

For an unknown sample spectrum x, the projection onto the PCA model of class g is calculated as

$$t_g = xP_g. \tag{9}$$

The reconstructed spectrum is

$$\hat{x}_g = t_g P_g^T. \tag{10}$$

The residual vector is then obtained as

$$e_g = x - \hat{x}_g. \tag{11}$$

The sample-to-model distance S_i, which measures how well a sample fits a class model, is calculated as

$$S_i = \sqrt{\frac{e_g e_g^{\mathrm{T}}}{p - a_g}} \tag{12}$$

where a_g represents the number of principal components retained in the class model.

Another important parameter is the sample leverage H_i, which measures how far the projected sample lies from the center of the PCA model:

$$H_i = t_g^{\mathrm{T}} \left(T_g^{\mathrm{T}} T_g \right)^{-1} t_g. \tag{13}$$

A sample is classified as belonging to class g if both of the following criteria are satisfied:

$$S_i \leq S_{\mathrm{crit},g} \tag{14}$$

$$H_i \leq H_{\mathrm{crit},g} \tag{15}$$

where $S_{\mathrm{crit},g}$ and $H_{\mathrm{crit},g}$ represent the critical limits determined from the training dataset at a selected confidence level.

The classification results can be visualized using Si–Hi plots, where samples falling within both limits are assigned to the corresponding material class.

In addition, the model-to-model distance between two SIMCA models provides a quantitative measure of separation between different material classes. Values significantly greater than 1 indicate that the classes are well separated and that the classification model has strong discrimination capability.

3.3. Chemometric software implementation

All chemometric calculations were performed using The Unscrambler (version 10.4, Camo Process AS).

PCA and SIMCA models were built using baseline-corrected fingerprint-region spectra from 650 to 1800 cm^{-1}. Three principal components were retained for modeling based on the cumulative explained variance shown in figure 6. For each modeled class, 30 spectra collected from five independently prepared cured package samples were used for training. Test validation used 15 spectra collected from five different independently prepared cured package samples. Thus, training and test spectra were separated at the physical package-sample level. In addition, 15 spectra from DA2 were used as an external unknown challenge set. DA2 was not included in model training and was used only to evaluate whether spectra from a material outside the modeled library would be rejected as unknown.

4. Results and discussion

4.1. Spectral characteristics of polymer materials

Representative FTIR-ATR spectra of the seven polymer materials analyzed in this study are shown in figure 5. The spectra were collected in the fingerprint region (1800–650 cm^{-1}), where characteristic vibrational modes of polymer functional groups are observed. The characteristic absorption bands observed in the polymer materials and their corresponding assignments are summarized in table 2.

Several common absorption bands appear across the spectra because most materials are based on epoxy or silicone polymer systems. A strong absorption band near 1720–1730 cm^{-1} corresponds to C=O stretching vibrations associated with carbonyl groups present in modified epoxy resins or additives. Peaks near 1600 cm^{-1} arise from aromatic C=C stretching in bisphenol-based epoxy structures. Bands observed around 1450 cm^{-1} are attributed to CH_2 deformation and C–O–H vibrations formed during epoxy curing reactions. Strong absorption features between 1270 and 1100 cm^{-1} correspond primarily to C–O–C stretching vibrations of ether linkages in cured epoxy networks. In addition, peaks around 1030–1100 cm^{-1} may include contributions from Si–O stretching associated with silica filler particles frequently used in packaging materials. Aromatic C–H out-of-plane bending vibrations are also observed near 800–750 cm^{-1}.

Despite these shared features, differences in peak intensity and band shape are observed among the materials. These variations reflect differences in resin composition, filler content, and curing chemistry, which provide distinctive spectral fingerprints that can be used for material identification.

4.2. Comparison of underfill, TIM, and DA materials

The four underfill materials exhibit similar spectral features due to their epoxy-based compositions, although variations in the 1100–1000 cm^{-1} region suggest differences in silica filler content and polymer formulation.

In contrast, the TIMs show dominant peaks associated with Si–O–Si stretching vibrations, indicating the presence of silicone-based polymer matrices. These spectra are characterized by strong absorption bands near 1070–1100 cm^{-1} and reduced aromatic bands compared with epoxy materials.

The DA adhesive exhibits spectral features typical of epoxy adhesives, including strong C–O–C stretching bands near 1250–1100 cm^{-1} and aromatic ring vibrations near 1600 cm^{-1}. However, the relative intensities of these peaks differ from those observed in underfill materials, reflecting differences in resin composition and filler systems.

These spectral differences provide the chemical basis for the multivariate classification analysis presented in the following sections.

4.3. FTIR spectral dataset and PCA dimensionality reduction

FTIR-ATR spectra collected from polymer materials in electronic packages contain hundreds of correlated spectral variables across the fingerprint region. To reduce dimensionality while retaining the most significant spectral information, PCA was applied to the dataset. The explained variance plot for the PCA model is shown below.

As illustrated in figure 6, the first principal component (PC1) explains approximately 57% of the total spectral variance, while the second principal component (PC2) contributes approximately 25%. The third principal component (PC3) explains an additional 11%, resulting in a cumulative explained variance of approximately 93% for the first three components.

Beyond the third principal component, additional components contribute only marginal improvements to the total variance. Therefore, the first three principal components were retained for further analysis and visualization. These results indicate that the majority of spectral information contained in the FTIR dataset can be represented in a reduced three-dimensional PCA space.

The PCA score plot using the first two principal components is shown in figure 7. Each point represents a spectrum obtained from a polymer material in an electronic package. The PCA score plot reveals clear clustering of different material categories, including UF, TIM, and DA.

The underfill materials UF1–UF4 form distinct clusters primarily distributed along the negative PC1 direction. TIMs TIM1 and TIM2 appear in the positive PC1 region, indicating strong spectral differences relative to the underfill materials. The DA forms a separate cluster, indicating unique spectral characteristics associated with its chemical composition.

Although some underfill clusters appear relatively close in the PCA score plot due to similarities in epoxy-based chemistry, they remain separable when higher principal components are considered.

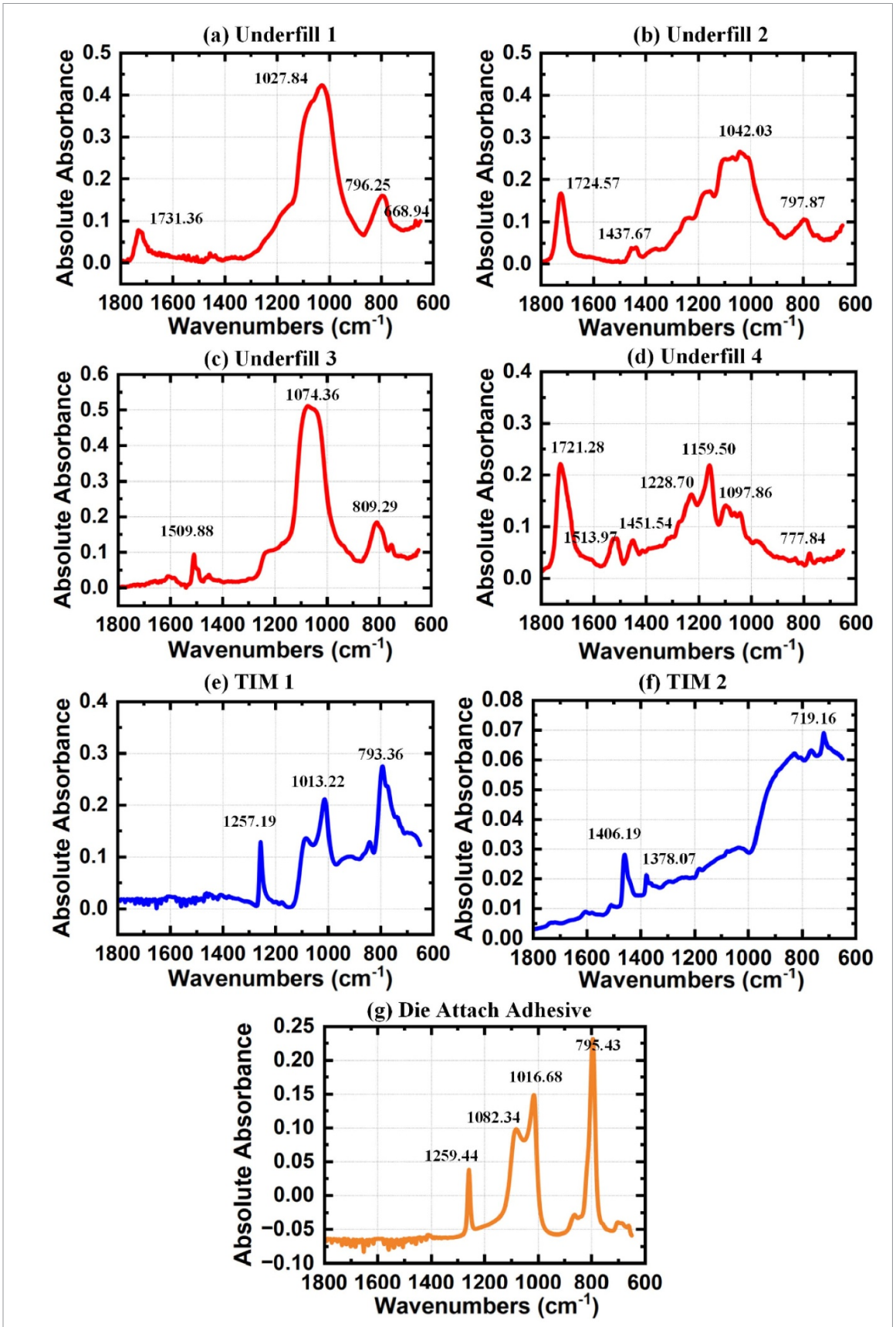

Figure 5. The average absorbance spectra of four underfill species, including (a) UF1, (b) UF2, (c) UF3, (d) UF4, (e) TIM1, (f) TIM2, (g) DA1 in the fingerprint region (650–1800 cm^{-1}) and their absorbance peak value.

Table 2. Characteristic FTIR absorption bands observed in polymer materials.

Wavenumber (cm^{-1})	Assignment	Functional group
1730	C=O stretching	Carbonyl groups
1660	C=O stretching	Conjugated carbonyl
1600	C=C stretching	Aromatic ring
1450	CH_2 deformation	C–O–H/methylene
1270	C–O stretching	Ether linkage
1100–1030	Si–O/C–O–C	Silica filler/epoxy
800–750	C–H bending	Aromatic ring

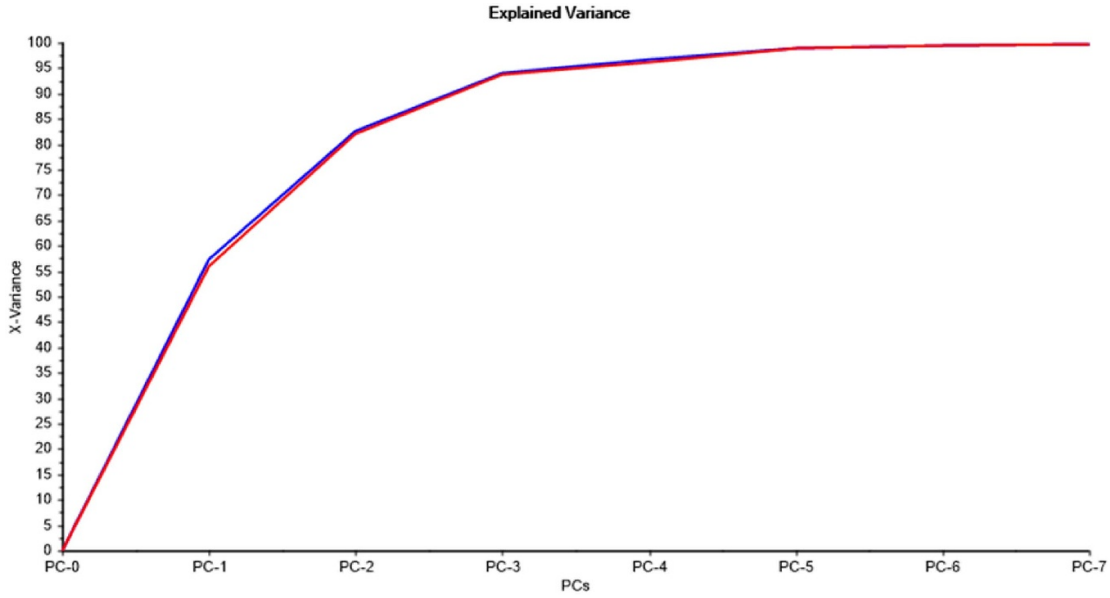

Figure 6. Total explained variance for PCA model.

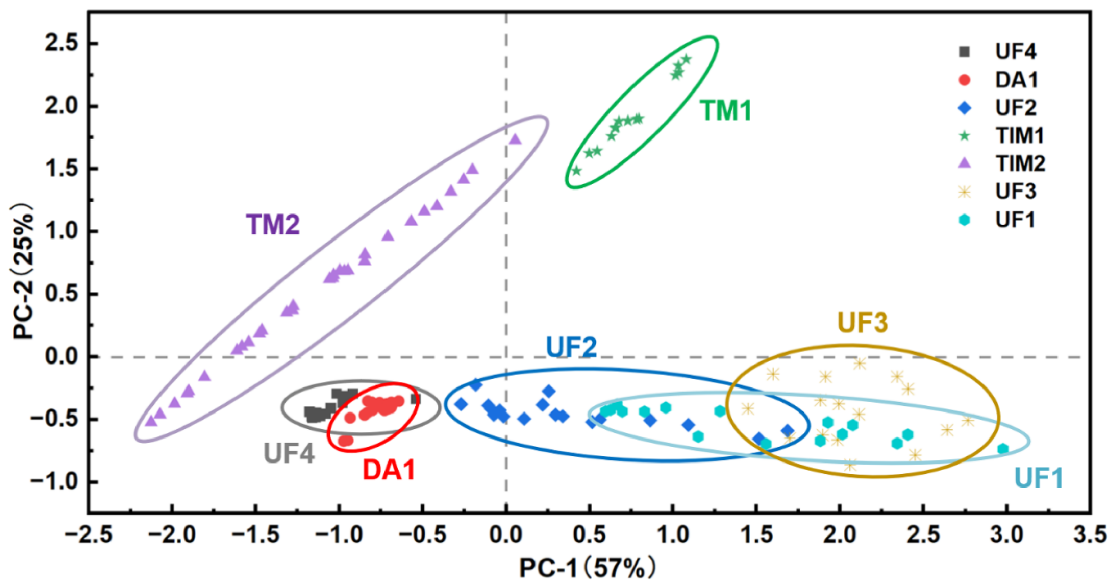

Figure 7. The PCA scores of the samples of seven polymers obtained from FTIR absorbance mode in the fingerprint region. (PC1 & PC2).

To further evaluate separation between different polymer materials, a three-dimensional PCA score plot was generated using the first three principal components as shown in figure 8. The three-dimensional PCA plot provides improved visualization of clustering relationships among the different

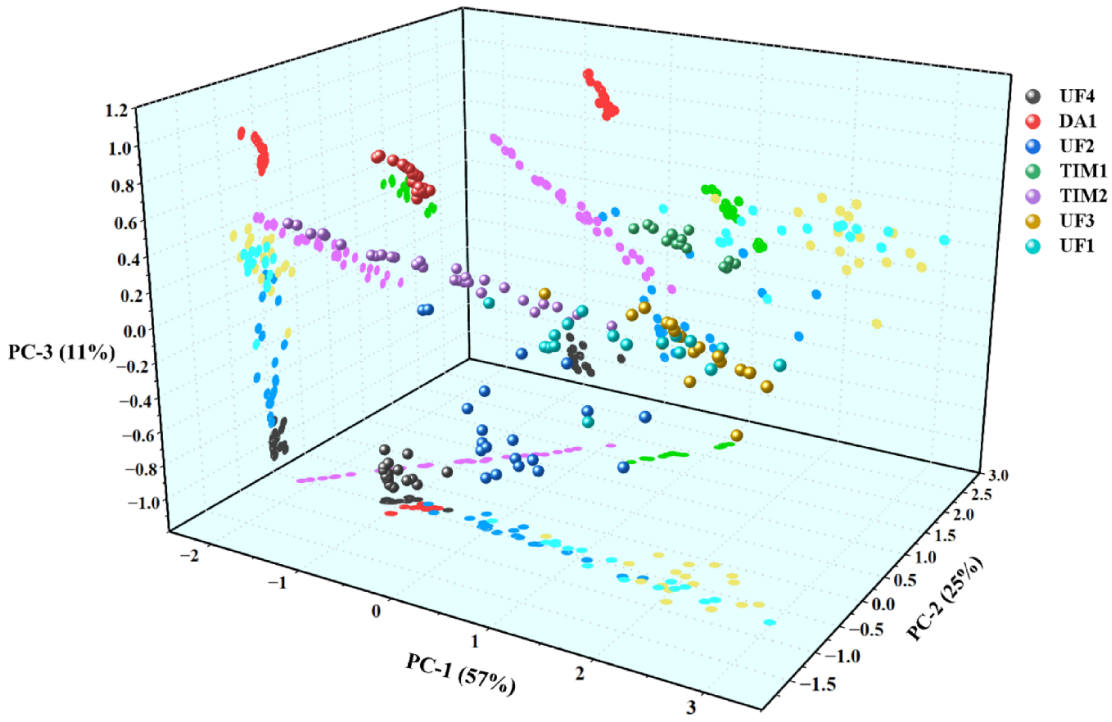

Figure 8. 3D PCA scores of the samples.

Table 3. SIMCA model-to-model distance.

Distance	UF1	UF2	UF3	UF4	TIM1	TIM2	DA1
UF1	1	19.0	39.3	115.9	459.4	370.8	185.9
UF2	19.0	1	113.6	66.1	1091.2	422.9	323.8
UF3	39.3	113.6	1	1975.3	3807.8	1619.3	2582.1
UF4	115.9	66.1	1975.3	1	3334.9	428.7	3191.7
TIM1	459.4	1091.2	3807.8	3334.9	1	250.7	5824.8
TIM2	370.8	422.9	1619.3	428.7	250.7	1	431.1
DA1	185.9	323.8	2582.1	3191.7	5824.8	431.1	1

material classes. The separation between underfill, TIM, and DA becomes more apparent when PC3 is included in the analysis.

The results confirm that FTIR-ATR spectra contain sufficient chemical information to differentiate between different categories of polymer materials used in electronic packaging.

To quantitatively evaluate the separation between material classes, SIMCA model-to-model distances were calculated. The resulting distance matrix is shown in table 3. In SIMCA analysis, a model-to-model distance greater than 3 is generally considered sufficient to indicate clear class separation. In the present dataset, all class distances significantly exceed this threshold, demonstrating strong separation among the different polymer materials. The largest distances are observed between TIMs and die attach, reflecting substantial chemical differences between these material types.

The confusion matrix in table 4 reports two validation outcomes: classification of test spectra from the seven modeled classes and rejection of the external unknown challenge material DA2. Because DA2 was not part of the modeled library, it is listed separately as an unknown challenge sample rather than as an eighth modeled class. This distinction is important because SIMCA is a class-modeling method: a spectrum may be accepted by a modeled class only when it satisfies the class distance and leverage limits; otherwise, it is rejected as unknown.

The modeled-class test set contained 105 spectra, of which 103 were correctly classified, giving an overall modeled-class accuracy of 98.1%. The external unknown challenge set contained 15 DA2 spectra, all of which were rejected as unknown. These results show that the SIMCA workflow can both classify spectra from the modeled library and reject a material outside the current library.

The only classification errors occurred between UF1 and UF2. These two materials are both epoxy-based underfill formulations and share similar absorption features associated with cured epoxy networks

Table 4. SIMCA discrimination result for test sets and external unknown challenge sample.

Samples \ SIMCA result	UF1	UF2	UF3	UF4	TIM1	TIM2	DA1	Unknown	Discrimination accuracy
UF1	15	0	1	0	0	0	0	0	93.3%
UF2	1	15	0	0	0	0	0	0	93.3%
UF3	0	0	15	0	0	0	0	0	100%
UF4	0	0	0	15	0	0	0	0	100%
TIM1	0	0	0	0	15	0	0	0	100%
TIM2	0	0	0	0	0	15	0	0	100%
DA1	0	0	0	0	0	0	15	0	100%
DA2	0	0	0	0	0	0	0	15	100% rejection

and silica-filled composite structures. In particular, the 1270–1000 cm^{-1} region contains overlapping contributions from C–O–C stretching in the epoxy network and Si–O–Si vibrations from silica filler. Although the SIMCA model-to-model distance between UF1 and UF2 is greater than the commonly used class-separation threshold, this metric describes the separation between class models rather than the position of every individual test spectrum. Spectra collected from heterogeneous underfill cross-sections can vary locally because of filler distribution, surface condition, and ATR contact. Therefore, individual UF1 or UF2 spectra near the acceptance boundary may be misclassified even when the average class models are well separated.

SIMCA was selected because the intended application is not only closed-set matching among known polymers but also rejection of spectra that do not belong to the modeled library. Simpler metrics such as Euclidean distance or cosine similarity are useful for spectral-library matching, but they normally assign an unknown spectrum to the nearest known class unless an additional rejection rule is defined. PLS-DA is also a discriminant method and requires representative examples of the classes expected during prediction. In contrast, SIMCA builds an independent PCA model for each material and evaluates both sample-to-model distance and leverage, which is appropriate when an unknown packaging polymer should be rejected rather than forced into the closest known class. The rejection of DA2 as an unknown material illustrates this class-modeling advantage.

The classification boundaries of the SIMCA models were evaluated using Si–Hi plots, which represent the sample-to-model distance S_i and leverage H_i of each sample relative to a specific class model. In SIMCA analysis, a sample is considered to belong to a given class when both parameters fall below their corresponding critical limits determined from the training dataset at the selected confidence level.

Three representative class models were evaluated, corresponding to DA, TIM, and UF. The resulting Si–Hi plots are shown in figures 9–11.

In the DA model, DA1 samples are located within the acceptance region defined by the critical limits, while samples from other material classes and the DA2 unknown challenge sample are rejected when they do not satisfy the class limits. This demonstrates that the spectral characteristics of the modeled DA are distinguishable from those of underfill and TIMs, while the class-modeling structure also allows spectra outside the modeled library to be treated as unknown.

The TIM model exhibits a well-defined acceptance region in which the TIM samples are clustered with relatively small residual distances. Samples belonging to other material classes show larger leverage values relative to the TIM model, reflecting significant differences in chemical composition. The clear separation observed in the Si–Hi space confirms that the SIMCA model effectively distinguishes TIM materials from other polymer types used in electronic packaging.

The underfill model also demonstrates strong classification capability. Most UF samples fall within the acceptance region defined by the model limits, while samples corresponding to other polymer materials lie outside the classification boundary. Although underfill materials share similar epoxy-based chemistries, the model successfully captures the spectral variations between different material categories.

5. Conclusions

This study developed a measurement framework for identifying polymer materials used in electronic packaging by combining micro-ATR FTIR spectroscopy with PCA and SIMCA chemometric analysis. The method was evaluated using package cross-sections containing four UF, two TIMs, and one DA

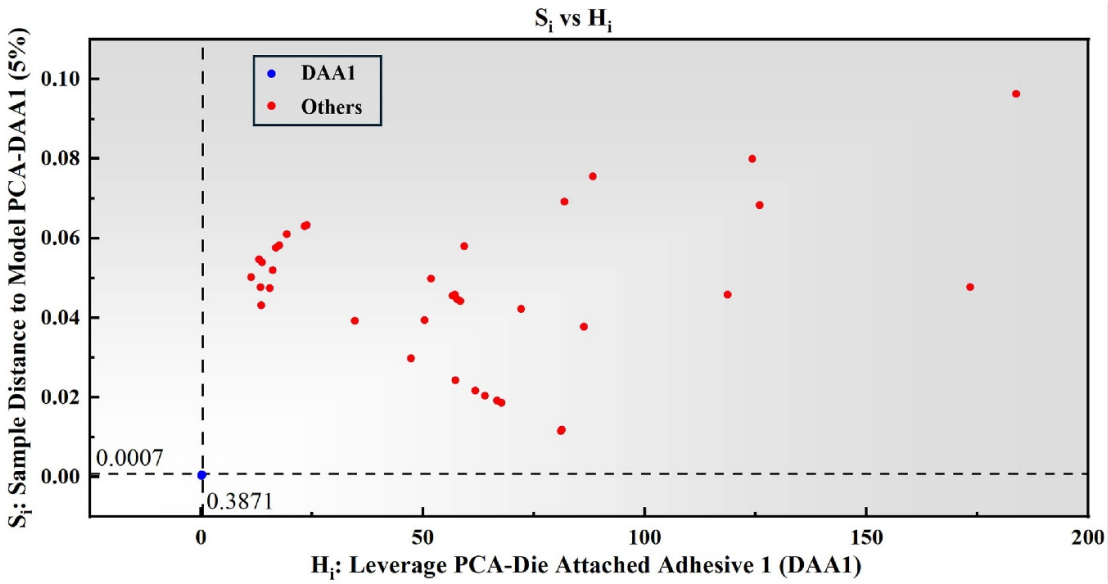

Figure 9. Si–Hi plot for the DA SIMCA model. The horizontal line represents the critical limit for the sample-to-model distance S_i, while the vertical line represents the leverage limit H_i.

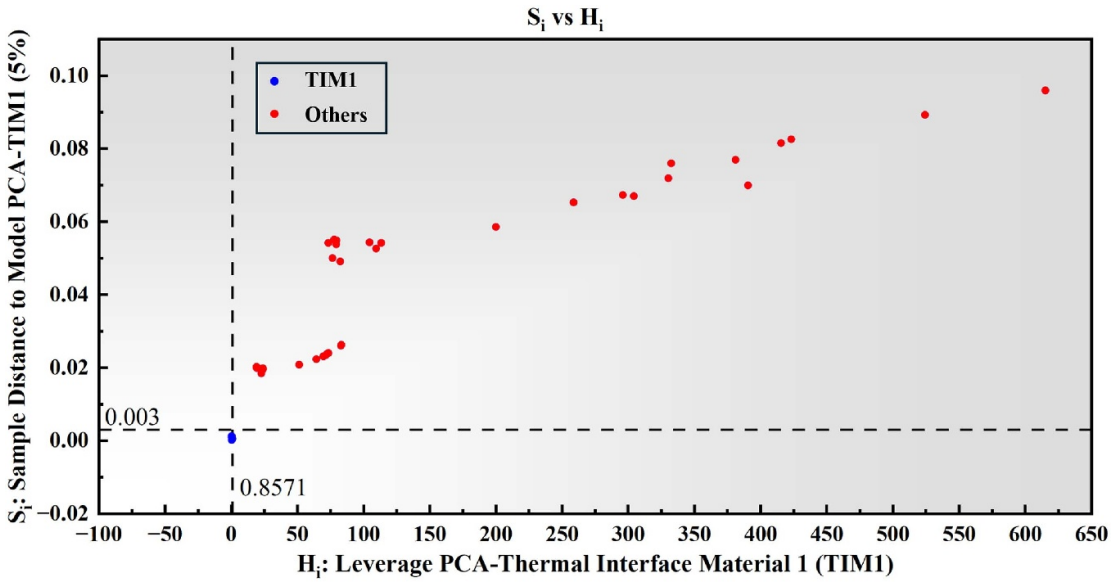

Figure 10. Si–Hi plot for the TIM SIMCA model.

adhesive as modeled classes, with a second DA adhesive reserved as an external unknown challenge sample.

PCA of the FTIR spectral dataset demonstrated that the first three principal components captured the majority of the spectral variance, with PC1, PC2, and PC3 explaining approximately 57%, 25%, and 11% of the total variance, respectively. The PCA score plots revealed clear clustering among different polymer material classes, indicating that FTIR-ATR spectra contain sufficient chemical information to differentiate between packaging materials.

SIMCA classification models were constructed for the seven modeled material classes. Training and test spectra were collected from different independently prepared cured package samples, which clarified the validation unit and reduced the risk of spectrum-level leakage between training and testing. The resulting model-to-model distance matrix showed separation between classes, while the confusion matrix showed that most modeled-class spectra were correctly classified and all DA2 spectra were rejected as unknown.

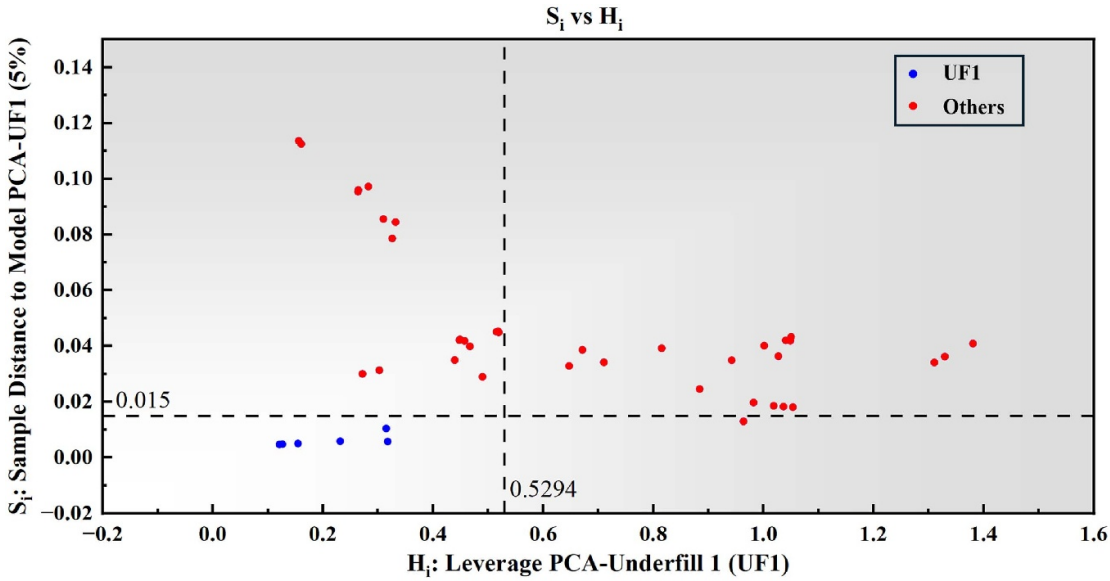

Figure 11. Si–Hi plot for the UF SIMCA model.

Classification performance was evaluated using a confusion matrix, which showed that nearly all samples were correctly classified into their respective material classes. The overall classification accuracy exceeded 98%, with only a small number of misclassifications occurring between chemically similar underfill materials.

The Si–Hi plots further showed that samples belonging to each modeled material class generally fall within the corresponding acceptance region, while spectra from other classes lie outside the classification boundary. These results support the feasibility of SIMCA class modeling for packaging-polymer identification, while also showing the importance of reporting class-specific errors and unknown rejection.

From a measurement perspective, several factors influencing the reliability of the FTIR-ATR identification method were discussed, including sample heterogeneity, ATR contact conditions, spectral acquisition parameters, and chemometric model construction. By carefully controlling these factors, the FTIR-ATR and SIMCA methodology can be implemented as a reproducible and traceable measurement approach.

Overall, the proposed framework provides a rapid and minimally destructive measurement workflow for identifying polymer materials in electronic-package cross-sections. The results should be interpreted as validation within the present material library rather than universal proof across all commercial packaging polymers. Additional DA adhesives, supplier lots, filler systems, and production-device samples are required before the method can be treated as broadly generalizable.

Future work will focus on expanding the spectral library to include additional polymer formulations, especially DA adhesives from different manufacturers and filler systems. Future studies will also compare SIMCA quantitatively with closed-set spectral matching and discriminant classifiers under independent-batch validation.

Data availability statement

All data that support the findings of this study are included within the article (and any supplementary files).

ORCID iDs

Junbo Yang 0000-0001-8301-1685
Yuhan Gao 0009-0003-0867-5344

References

[1] Plachy Z, Prazanova A, Dusek K and Geczy A 2025 Underfill: a review of reliability improvement methods in electronics production *Polym. (Basel)* **17** 2206

[2] Wan Y J, Li G, Yao Y M, Zeng X L, Zhu P L and Sun R 2020 Recent advances in polymer-based electronic packaging materials *Compos. Commun.* **19** 154–67

[3] Li Z Y, Chen X, Liu D, Zhou Y L, Pan D and Shin S M 2025 Recent advances in polymer-based composites for thermal management and electromagnetic wave absorption *Adv. Compos. Hybrid Mater.* **8** 210

[4] Gao Y H, Chen Y X, Yu Z N, Xu K Z, Wang C J, Xie J G, Zhou Y Q, Lei X and Zhu F L 2025 *In-situ* measurement method for warpage of electronic package substrate based on speckle-free DIC and carbon coating *Int. Conf. on Electronic Packaging Technology* (IEEE)

[5] Cai C Y, Pan K, Yang J B and Park S 2020 Comparative analysis of package warpage using confocal method and digital image correlation *Int. Society Conf. on Thermal and Thermomechanical Phenomena in Electronic Systems* pp 945–9

[6] Gao Y H, Xiong C G, Lv W S, Xu K Z, Lei X and Zhu F L 2024 *In situ* warpage measurement of electronic packages with projected speckle DIC and deep learning-based ROI identification *IEEE Trans. Instrum. Meas.* **73** 1–9

[7] Gao Y H, Chen Y X, Yu Z N, Xiong C G, Lei X, Lv W S, Liu S and Zhu F L 2024 Correction of thermal airflow distortion in warpage measurements of microelectronic packaging structures via deep learning-based digital image correlation *Microsyst. Nanoeng.* **10** 118

[8] Yegin C *et al* 2017 Metal–organic–inorganic nanocomposite thermal interface materials with ultralow thermal resistances *ACS Appl. Mater. Interfaces* **9** 10120–7

[9] Wang Y K, Liu H Z, Huo L H, Li H B, Tian W C, Ji H Y and Chen S 2024 Apr Research on the reliability of advanced packaging under multi-field coupling: a review *Micromachines* **15** 422

[10] Bender E, Bernstein J B and Boning D S 2024 Modern trends in microelectronics packaging reliability testing *Micromachines* **15** 398

[11] Wen Y F, Chen C, Ye Y S, Xue Z G, Liu H Y, Zhou X P, Zhang Y, Li D Q, Xie X L and Mai Y W 2022 Dec Advances on thermally conductive epoxy-based composites as electronic packaging underfill materials-a review *Adv. Mater.* **34** 2201023

[12] Ng F C and Abas M A 2022 Underfill flow in flip-chip encapsulation process: a review *J. Electron. Packag.* **144** 010803

[13] Guo J F, Su C, Liu J, Cheng J, Zhang J Y and Gao F 2024 Construction of silver-epoxy adhesive with suppressed silver migration rate based on thiol-silver interaction *Polymer* **300** 126959

[14] Alim M A, Abdullah M Z, Aziz M S A, Kamarudin R and Gunnasegaran P 2021 Recent advances on thermally conductive adhesive in electronic packaging: a review *Polymers* **13** 3337

[15] Xing W K, Xu Y, Song C Y and Deng T 2022 Recent advances in thermal interface materials for thermal management of high-power electronics *Nanomaterials* **12** 3365

[16] Xie X C, Pang Y S, Rao S P, Zeng C, Zhang L C, Zhang C X, Guo S F, Xu J B, Zeng X L and Sun R 2024 Thermal interface materials with high adhesion and enhanced thermal conductivity via optimization of polydimethylsiloxane networks and aluminum fillers *ACS Appl. Polym. Mater.* **6** 12765–73

[17] Yang J B, Lai Y Y, Pan K, Xu J F, Mikjaniec T, Cain S, Park S and Soc I C 2021 A comparison study of TIM degradation of phase change material and thermal grease *Electronic Components and Technology Conf.* pp 1978–83

[18] Yang J, Cai C, Yin P, Pan K, Lai Y, Wang J and Park S 2022 Optimal thermo-mechanical reliability design of 2.5D lidless package *2022 21st IEEE Intersociety Conf. on Thermal and Thermomechanical Phenomena in Electronic Systems (Itherm)* pp 1–6

[19] Wang J, Niu Y L, Park S and Yatskov A 2018 Modeling and design of 2.5D package with mitigated warpage and enhanced thermo-mechanical reliability *Electronic Components and Technology Conf.* (IEEE) pp 2477–83

[20] Schäfer T, Buntkowsky G and Gutmann T 2020 Solid-state nuclear magnetic resonance as a versatile tool to identify the main chemical components of epoxy-based thermosets *ACS Omega* **5** 5412–20

[21] Gnoffo C and Frache A 2024 Jan Identification of plastics in mixtures and blends through pyrolysis-gas chromatography/mass spectrometry *Polymers* **16** 71

[22] Sorolla-Rosario D, Llorca-Porcel J, Pérez-Martínez M, Lozano-Castelló D and Bueno-López A 2022 Study of microplastics with semicrystalline and amorphous structure identification by TGA and DSC *J. Environ. Chem. Eng.* **10** 106886

[23] Kaur H, Rana B, Tomar D, Kaur S and Jena K C 2021 Fundamentals of ATR-FTIR spectroscopy and its role for probing *in-situ* molecular-level interactions *Modern Techniques of Spectroscopy: Basics, Instrumentation, and Applications* ed D K Singh, M Pradhan and A Materny (Springer) pp 3–37

[24] Koczon P, Holaj-Krzak J T, Palani B K, Bolewski T, Dabrowski J, Bartyzel B J and Gruczynska-Sekowska E 2023 The analytical possibilities of FT-IR spectroscopy powered by vibrating molecules *Int. J. Mol. Sci.* **24** 1013

[25] Souza A S, Bezerra M A, Cerqueira U, Rodrigues C J O, Santos B C, Novaes C G and Almeida E R V 2024 An introductory review on the application of principal component analysis in the data exploration of the chemical analysis of food samples *Food Sci. Biotechnol.* **33** 1323–36

[26] Beattie J R and Esmonde-White F W L 2021 Exploration of principal component analysis: deriving principal component analysis visually using spectra *Appl. Spectrosc.* **75** 361–75

[27] Rácz A, Gere A, Bajusz D and Héberger K 2018 Is soft independent modeling of class analogies a reasonable choice for supervised pattern recognition? *RSC Adv.* **8** 10–21

[28] Kucheryavskiy S, Rodionova O and Pomerantsev A 2024 A comprehensive tutorial on data-driven SIMCA: theory and implementation in web *J. Chemom.* **38** e3556

[29] Pagani A P, Camargo G, Ibañez G A, Olivieri A C, Pomerantsev A L and Rodionova O Y 2024 Data-driven version of multiway soft independent modeling of class analogy (N-Way DD-SIMCA): theory and application *Anal. Chem.* **96** 4845–53

[30] Deconinck E, Duchateau C, Balcaen M, Gremeaux L and Courselle P 2022 Chemometrics and infrared spectroscopy—a winning team for the analysis of illicit drug products *Rev. Anal. Chem.* **41** 228–55

[31] Zhang W Q, Yin L, Zhao M, Tan Z Y and Li G Y 2021 Rapid and non-destructive quality verification of epoxy resin product using ATR-FTIR spectroscopy coupled with chemometric methods *Microchem. J.* **168** 106397

[32] da Silva D J and Wiebeck H 2022 ATR-FTIR spectroscopy combined with chemometric methods for the classification of polyethylene residues containing different contaminants *J. Polym. Environ.* **30** 3031–44

[33] Yang J B, Xu J F and Park S 2020 Identification of polymer materials in electronic packages including counterfeit prevention *Electronic Components and Technology Conf.* (IEEE) pp 2317–24

[34] Tummino M L, Chrimatopoulos C, Bertolla M, Tonetti C and Sakkas V 2023 Configuration of a simple method for different polyamides 6.9 recognition by ATR-FTIR analysis coupled with chemometrics *Polymers* **15** 3166
[35] Tan A L, Zhao J, Zhao Y, Li X H and Su H J 2023 Determination of microplastics by FTIR spectroscopy based on quaternion parallel feature fusion and support vector machine *Chemom. Intell. Lab. Syst.* **243** 105018
[36] da Silva V H, Murphy F, Amigo J M, Stedmon C and Strand J 2020 Classification and quantification of microplastics (<100 μm) using a focal plane array-Fourier transform infrared imaging system and machine learning *Anal. Chem.* **92** 13724–33
[37] Nguyen T, Shamsabadi A A and Bavarian M 2023 Coupling ATR-FTIR spectroscopy with multivariate analysis for polymers manufacturing and control of polymers' molecular weight *Digit. Chem. Eng.* **7** 100089
[38] Kozloski R, Cowger W and Arienzo M M 2024 Moving toward automated μFTIR spectra matching for microplastic identification: addressing false identifications and improving accuracy *Microplast. Nanoplast.* **4** 27
[39] Willans M, Szczecinski E, Roocke C, Williams S, Timalsina S, Vongsvivut J, McIlwain J, Naderi G, Linge K L and Hackett M J 2023 Development of a rapid detection protocol for microplastics using reflectance-FTIR spectroscopic imaging and multivariate classification *Environ. Sci. Adv.* **2** 663–74
[40] Tarhan I and Kestek H M 2024 Investigation of new analysis methods for simultaneous and rapid identification of five different microplastics using ATR-FTIR spectroscopy and chemometrics *Environ. Pollut.* **362** 125043
[41] Yan X, Cao Z, Murphy A, Ye Y, Wang X and Qiao Y 2023 FRDA: fingerprint region based data augmentation using explainable AI for FTIR based microplastics classification *Sci. Total Environ.* **896** 165340
[42] Huang Y, Bigio D and Pecht M G 2004 Fill pattern and particle distribution of underfill material *IEEE Trans. Compon. Packag. Technol.* **27** 493–8
[43] Li Y, Zhong C, Peng X, Li C, Jiang R, Lu J and Sun R 2022 Capillary flow analysis of underfill in flip-chip package *2022 23rd Int. Conf. on Electronic Packaging Technology (ICEPT)* pp 1–5
[44] Ng F C, Abas A, Gan Z L, Abdullah M Z, Ani F C and Ali M Y T 2017 Discrete phase method study of ball grid array underfill process using nano-silica filler-reinforced composite-encapsulant with varying filler loadings *Microelectron. Reliab.* **72** 45–64